



UNIVERSIDAD DE INVESTIGACIÓN DE TECNOLOGÍA EXPERIMENTAL YACHAY

Escuela de Ciencias Físicas y Nanotecnología

TÍTULO: Fabrication of Zinc Oxide Films Using Spray Pyrolysis Method

Trabajo de integración curricular presentado como requisito para la
obtención del título de Ingeniero en Nanotecnología

Autor:

Revelo Muñoz David Alejandro

Tutor:

Ph.D. Bramer Escamilla Werner

Urcuquí, Julio 2020

SECRETARÍA GENERAL
(Vicerrectorado Académico/Cancillería)
ESCUELA DE CIENCIAS FÍSICAS Y NANOTECNOLOGÍA
CARRERA DE NANOTECNOLOGÍA
ACTA DE DEFENSA No. UITEY-PHY-2020-00015-AD

A los 22 días del mes de julio de 2020, a las 15:00 horas, de manera virtual mediante videoconferencia, y ante el Tribunal Calificador, integrado por los docentes:

Presidente Tribunal de Defensa	Dra. BRICEÑO ARAUJO, SARAH ELISA , Ph.D.
Miembro No Tutor	Dr. REINOSO CARLOS , Ph.D.
Tutor	Dr. BRAMER ESCAMILLA , WERNER , Ph.D.

El(la) señor(ita) estudiante **REVELO MUÑOZ, DAVID ALEJANDRO**, con cédula de identidad No. **1804452553**, de la **ESCUELA DE CIENCIAS FÍSICAS Y NANOTECNOLOGÍA**, de la Carrera de **NANOTECNOLOGÍA**, aprobada por el Consejo de Educación Superior (CES), mediante Resolución **RPC-SO-13-No.156-2015**, realiza a través de videoconferencia, la sustentación de su trabajo de titulación denominado: **Fabrication of Zinc Oxide Films Using Spray Pyrolysis Method**, previa a la obtención del título de **INGENIERO/A EN NANOTECNOLOGÍA**.

El citado trabajo de titulación, fue debidamente aprobado por el(los) docente(s):

Tutor	Dr. BRAMER ESCAMILLA , WERNER , Ph.D.
--------------	---------------------------------------

Y recibió las observaciones de los otros miembros del Tribunal Calificador, las mismas que han sido incorporadas por el(la) estudiante.

Previamente cumplidos los requisitos legales y reglamentarios, el trabajo de titulación fue sustentado por el(la) estudiante y examinado por los miembros del Tribunal Calificador. Escuchada la sustentación del trabajo de titulación a través de videoconferencia, que integró la exposición de el(la) estudiante sobre el contenido de la misma y las preguntas formuladas por los miembros del Tribunal, se califica la sustentación del trabajo de titulación con las siguientes calificaciones:

Tipo	Docente	Calificación
Miembro Tribunal De Defensa	Dr. REINOSO CARLOS , Ph.D.	8,7
Presidente Tribunal De Defensa	Dra. BRICEÑO ARAUJO, SARAH ELISA , Ph.D.	8,0
Tutor	Dr. BRAMER ESCAMILLA , WERNER , Ph.D.	9,6

Lo que da un promedio de: **8.8 (Ocho punto Ocho)**, sobre 10 (diez), equivalente a: **APROBADO**

Para constancia de lo actuado, firman los miembros del Tribunal Calificador, el/la estudiante y el/la secretario ad-hoc.

Certifico que en cumplimiento del Decreto Ejecutivo 1017 de 16 de marzo de 2020, la defensa de trabajo de titulación (o examen de grado modalidad teórico práctica) se realizó vía virtual, por lo que las firmas de los miembros del Tribunal de Defensa de Grado, constan en forma digital.

REVELO MUÑOZ, DAVID ALEJANDRO
Estudiante

Dra. BRICEÑO ARAUJO, SARAH ELISA , Ph.D.
Presidente Tribunal de Defensa

Dr. BRAMER ESCAMILLA , WERNER , Ph.D.
Tutor

Dr. REINOSO CARLOS , Ph.D.
Miembro No Tutor

CIFUENTES TAFUR, EVELYN CAROLINA
Secretario Ad-hoc

AUTORÍA

Yo, **DAVID ALEJANDRO REVELO MUÑOZ**, con cédula de identidad 180445255-3, declaro que las ideas, juicios, valoraciones, interpretaciones, consultas bibliográficas, definiciones y conceptualizaciones expuestas en el presente trabajo; así cómo, los procedimientos y herramientas utilizadas en la investigación, son de absoluta responsabilidad de el/la autora (a) del trabajo de integración curricular. Así mismo, me acojo a los reglamentos internos de la Universidad de Investigación de Tecnología Experimental Yachay.

Urcuquí, julio 2020.



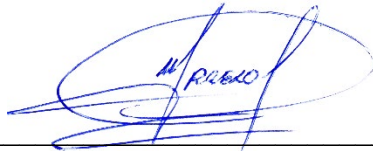
David Alejandro Revelo Muñoz
CI: 180445255-3

AUTORIZACIÓN DE PUBLICACIÓN

Yo, **DAVID ALEJANDRO REVELO MUÑOZ**, con cédula de identidad 180445255-3, cedo a la Universidad de Tecnología Experimental Yachay, los derechos de publicación de la presente obra, sin que deba haber un reconocimiento económico por este concepto. Declaro además que el texto del presente trabajo de titulación no podrá ser cedido a ninguna empresa editorial para su publicación u otros fines, sin contar previamente con la autorización escrita de la Universidad.

Asimismo, autorizo a la Universidad que realice la digitalización y publicación de este trabajo de integración curricular en el repositorio virtual, de conformidad a lo dispuesto en el Art. 144 de la Ley Orgánica de Educación Superior

Urcuquí, julio 2020.



David Alejandro Revelo Muñoz
CI: 180445255-3

Dedicatoria

A mis padres, hermana y amigos (hinchada toxica) por su apoyo incondicional en el camino para alcanzar mis metas.

David Alejandro Revelo Muñoz

Agradecimiento

Me gustaría expresar mi gratitud a todas las personas que me ayudan durante el proceso de investigación y escritura. Un agradecimiento especial a mi tutor, PhD. Werner Bramer Escamilla, por ser mi guía durante el desarrollo de esta investigación, y por su paciencia, motivación e inmenso conocimiento.

Además, me gustaría agradecer a mis padres, Pablo Revelo Martínez y Luisa Muñoz Sánchez, por apoyarme durante toda mi vida.

A Yachay Tech University por ser mi hogar durante los últimos cinco años y por sus increíbles profesores.

David Alejandro Revelo Muñoz

Resumen

En las últimas décadas, las energías limpias y renovables han sido uno de los temas más relevantes debido a la continua demanda de energía en todo el mundo. Según U.S. Energy Information Administration (EIA) en su informe de 2019, la energía renovable se convertirá en la principal fuente de consumo de energía para 2050 y la energía solar dominará la generación renovable para ese año. Este trabajo describe la fabricación de películas de óxido de zinc y de óxido de zinc dopadas con boro mediante el método de pirólisis depositadas sobre un sustrato de vidrio con posibles aplicaciones en células solares fotovoltaicas. Se describen medidas ópticas y eléctricas para la caracterización de películas de ZnO. Usando el método de diagrama de Tauc, se confirmó la deposición de semiconductores de óxido de zinc en base a su separación de banda óptica. Se aplicaron mediciones de cuatro puntas para conocer su conductividad eléctrica. Se obtuvieron películas semiconductoras de óxido de zinc transparentes con $6,7 \text{ k}\Omega$ de resistencia de lámina como el valor más bajo para películas dopadas con boro y se obtuvieron diferentes valores de banda óptica dependiendo del nivel de dopaje. Se describen las características de las películas de óxido de zinc a diferentes porcentajes de peso de boro dopado tales como transparencia, conductividad eléctrica. En este trabajo obtuvieron películas reproducibles con gran separación de banda óptica y alto porcentaje de transmisión.

Palabras Clave: Película monocapa, ZnO dopado con boro, gráfico de Tauc, mediciones a cuatro puntas, semiconductor

Abstract

In the last decades, clean and renewable energies have been one of the most relevant topics due to the continues demand of energy around the world. According to U.S. Energy Information Administration (EIA) in its report of 2019, renewable energy becomes the leading source of energy consumption by 2050 and solar energy will dominate renewable generation for that year. This work describes the fabrication of zinc oxide and zinc oxide boron doped films by spray pyrolysis method in a glass substrate with possible applications in photovoltaics solar cells. Optical and electrical measurements are described for the characterization of ZnO films. Using Tauc plot method the deposition of zinc oxide semiconductor was confirmed based on its optical band gap. Four probe measurements were applied in order to know its electrical conductivity. Transparent zinc oxide semiconductor films were obtained with 6.7 k Ω of sheet resistance as the lowest value for boron doped films and different optical band gaps were obtained depending of the doping level. The characteristics of zinc oxide films at different wt% boron doped such as transparency, electrical conductivity are described. Reproducible films were obtained with large optical band gap and high transmission percentage.

Keywords: Monolayer film, boron doped ZnO, Tauc plot, four probe measurements, semiconductor

Contents

List of Figures	viii
List of Tables	ix
0.1 Problem Statement	5
0.2 General and Specific Objectives	5
0.2.1 General Objectives	5
0.2.2 Specific Objectives	5
1 Theoretical Background	7
1.1 Solar panels	7
1.2 Photovoltaics	7
1.3 Optical band gap	9
1.4 Spray pyrolysis method	10
1.5 Two point versus four point probe	10
1.6 Tauc plot	12
2 Methodology	15
2.1 Spray Pyrolysis Method for Fabrication of Transparent Conductive Glass Films	15
2.2 Four point probe measurements	16
2.3 Measurements of optical band gap using Tauc plot method	18
3 Results & Discussion	21
3.1 Band Gap Obtained by Tauc Plot Method	21
3.2 Transmission measurements	23
3.3 Sheet resistance values	24
4 Conclusions & Outlook	29
Bibliography	31

List of Figures

1	Ecuador renewable power capacity	2
2	Zinc oxide crystal structures	4
1.1	Solar panels	8
1.2	Simple photovoltaic cell	8
1.3	Electronic band structure	9
1.4	Diagram of spray pyrolysis method	10
1.5	Two-point probe arrangement	11
1.6	Direct and indirect transition	13
2.1	Burner for deposition	16
2.2	Four-point probe arrangement	17
2.3	Four-point probe device	17
2.4	Sections of the deposited film	18
2.5	UV-vis device	19
3.1	Tauc plot for boron doped zinc oxide films	22
3.2	Optical Transmission	24
3.3	ZnO and ZnO boron doped films	25
3.4	Sheet Resistance at different doping levels	26

List of Tables

1	Zinc oxide properties	4
1.1	Nature of electronic transitions	12
3.1	Films sheet resistance values of each deposited film	24
3.2	Standard Deviation Values for Sheet Resistances Measurements	25

Introduction

A large increase in energy demand in the last decades by the "modern life style", and the rise of energy prices in the beginning of the twenty first century have created a need to work in the development of clean and renewable energy sources (Suganthi & Samuel, 2012). At the moment, one of the branches of the industry with high growth and the most interest is the solar energy conversion, specifically photovoltaic (PV) (Petrova-Koch, Hezel, & Goetzberger, 2020). This as a result of its large potential to be used everywhere on the globe compared with other renewable energy sources like wind or water, low operating cost and pollution free (Bhatia, 2014).

In the last two decades, a fast growth demand have been seen in the PV market. However, many solar roofs and markets still having PV first-generation ("Engineered Nanomaterials for Energy Applications," 2018). Petrova-Koch, Hezel, and Goetzberger (2020) mentioned that, "this generation is characterized by relatively low efficiencies of the cells and modules". Additionally, these PV first generation are based mainly on wafers with really high cost materials. So, even that the cost of PV in the past years has dropped, the actual price is still relatively high (Bhatia, 2014). Thus, due to the high demand on the PV market, new innovative solutions based on new materials are searched. Such solutions are mainly focused into reduce the application of expensive semiconductor materials. The solution that appears are called second generation PV, based on thin-film PV technology ("Engineered Nanomaterials for Energy Applications," 2018).

Since the invention of the first solar cell in 1950s, the search of new materials for the fabrication of cost-effective photovoltaics is still in process. For solar energy conversion a photovoltaic heterojunction is required. Such heterojunction consist of two different semiconductor layers n-type and p-type. These semiconductor materials require a band gap large enough to be transparent to most of the useful solar spectrum to be employed in photovoltaics (Aranovich, Ortiz, & Bube, 1979). Currently, the most common transparent conductor is based on tin-doped indium oxide (ITO) film, as it has good transmittance in the visible range and superior electrical resistivity (Gordon, 1997). Despite this, due to the difficult in extraction and rise in demand, ITO represents a high cost in applications to photovoltaics. So, several alternatives technologies to ITO have been presented finding a cost-efficient reduction during the pass of the years (Scharber et al., 2006).

In some countries like Germany, Spain and Japan, the PV market has increased rapidly in the last 5 year. In the case of Germany where although is not the sunniest part of Europe, German market, nowadays is comparable to Japan, which is the biggest PV producer worldwide (Bhatia, 2014). This result is attributed to the joint of efforts of politics, industry, and academia. The most influence case it is the promotion of the RES law (EEG in German)

and the preferential feed-in tariff for solar electricity. These policies also have influenced many other countries to support the development of targets for clean energy (Petrova-Koch, Hezel, & Goetzberger, 2020).

Situation of Alternative energy sources in Ecuador

In Ecuador, the organism responsible for regulating and planing the entire power sector of the country, and with the responsibility to promote renewable energy sources is the Ministry of Electricity and Renewable Energy (Ministerio de Electricidad y Energía Renovable-MEER). In the past "Electric Law" of 1996, the National Electric Council (CONELEC) was the organism which regulated and promoted renewable energies. During 2000 to 2015, Ecuador had a feed-in tariff system to support the implementation of renewable electricity. Through the time, this system suffered many changes. To cite some cases, in 2000 Regulation CONELEC 008/00 established a 10 year feed-in tariff for wind, solar PV, biomass and biogas, and geothermal, with a limit of 15MW per project. Other important change, in 2006 rates were adjusted by Regulation CONELEC 009/06, notably for solar PV. Another adjusted was in 2013, where Regulation CONELEC 001/13 did not maintain solar PV under the feed-in tariff. Now, CONELEC was disbanded and new laws were developed with preferential regulations for renewable energy by the Regulatory and Control Electricity Agency (ARCONEL) (IRENA, 2015). In Fig. 1, a representation of renewable energy capacity evolution of Ecuador per year since 2000 to 2013.

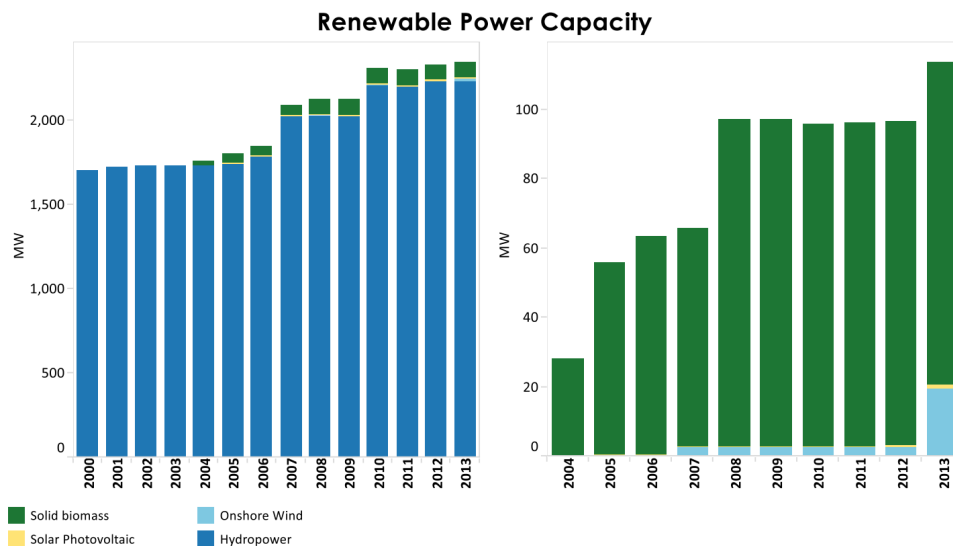


Figure 1: Ecuador renewable power capacity per year since 2000 to 2013 in MW based on different energy sources. In blue, hydropower; in green, solid biomass; yellow, solar photovoltaic; and light blue, onshore wind. Reprinted from Renewable Energy Policy Brief: Ecuador, 2015.

Actually, in Galapagos there is the initiative "Galapagos Island Zero Fossil Fuels" with the objective to boost

renewable energy projects and displace oil-based electricity generation. As result of this initiative, two wind farms, two PV projects and two hybrid PV-biofuel-battery projects are being developed with assistance from Korea (KOICA), Japan (JICS) and Germany (KfW). Furthermore, since 2015, rural electrification projects are prioritized by the government due to the Electric Law, where, additionally, must be provided for them from the general budget, while allowing contributions from other public and private entities. At the moment, Ecuador has projects focused to increase access to electricity in isolates areas to families in communities such as the Ecuadorian Amazon Region (IRENA, 2015).

Properties of Zinc Oxide layer and required properties for Solar Cell applications

For solar PV applications several structures of transparent conductive oxide (TCO) have been proposed in order to enhance TCO properties, among these are TCO/Metal/TCO and TCO/TCO (Calnan & Tiwari, 2010). In solar cells application, oxide layers must have certain characteristics to be optimal. Such characteristics are excellent electrical conductivity and optical transparency in visible range of electromagnetic spectrum (Murugesan, Arjunraj, Mayandi, Venkatachalapathy, & Pearce, 2018).

Several researches have been reported about TCO showing great results in electrical conductivity and transparency for aluminum, indium or gallium doped films (Hosono, 2013). Between these, Gordon (1997) describes good properties for PV applications of zinc oxide (ZnO) conductive films doped by boron, gallium, aluminum, indium and fluorine. ZnO is a wide band gap semiconductor and it has many attractive features, among these, there are the facility to be grown by a variety of low cost different methods and a large variety of nanostructured morphologies (Djurišić, Liu, & Leung, 2014).

ZnO is a semiconductor material of great interest for the fabrication of optoelectronic devices (Hosono, 2013). Generally, ZnO has a wide and direct bandgap (3.437 eV at 2 K). Intrinsically, this compound is deposited as an n-type material due to the presence of intrinsic defects (oxygen vacancies and zinc interstitials) and the presence of impurities in the form of hydrogen (Nagar & Chakrabarti, 2017). It has a large exciton-binding energy of 60 meV compared with GaN: 21-25 meV. The crystal structure of ZnO is hexagonal wurtzite (each anion is surrounded by four cations), zinc blend and rock salt, Figure 2. Among these, wurtzite structure is the thermodynamically stable phase in ambient conditions (Nagar & Chakrabarti, 2017). In Figure 2 is shown the wurtzite structure, this structure is composed by two hexagonal close packed sub-lattices. Among other properties, ZnO is insoluble en water and alcohol, it can be dissolved in dilute acids and its melting point is 1975 °C. A summary of the properties of ZnO are listed in Table 1 (Nagar & Chakrabarti, 2017).

In photovoltaics, some possible applications of ZnO are reported by Djurišić, Liu, and Leung (2014), such as anti-reflection layer, light-trapping coating and as contact. Typically, ZnO exhibits n-type conductivity with applications as a conductive contact oxide in solar cells. However, for the use of ZnO as TCO in photovoltaics doping is necessary. Generally, the dopants used are elements from the group III (Al, Ga and In) and group VII (Cl and I). Nevertheless, the use of indium as a doping agent for zinc oxide it is not of interest since there is not

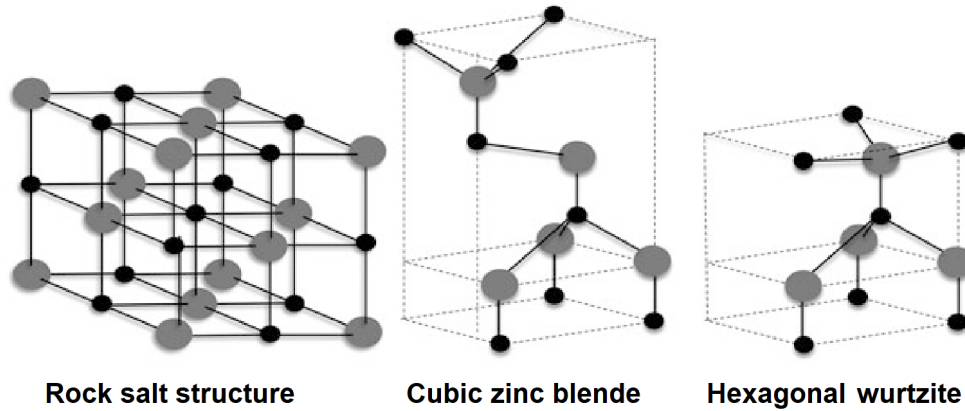


Figure 2: Representation of ZnO crystal structures. The gray spheres represents zinc atoms and black spheres oxygen atoms. Reprinted from Optimisation of ZnO Thin Films, by Nagar and Chakrabarti, 2017.

Properties	Specifications	Comments
Structure	Wurzite	Same as hexagonal
Band gap	3.3 eV	Wide band gap semiconductor
Exciton-binding energy	60 meV	Higher than GaN (21-25 meV)
Piezoelectricity	1.2 cm^{-2}	Highest among all semiconductors
Hardness	$\sim 5 \Omega$	For single crystal
Toxicity	Very low	Same as other compound semiconductors

Table 1: Properties of zinc oxide

significant advantages over commonly used ITO electrodes (Djurišić, Liu, & Leung, 2014).

It was also reported by Sutradhar and Saha (2016) a synthesis of ZnO nanoparticles for photovoltaic application. In their report, ZnO semiconductor with a direct wide band gap (3.2-3.37 eV) and good transparency ($\geq 80\%$) at room temperature are described. As well, it is mentioned the ZnO as an alternating material for TiO_2 due to its stability, environment friendliness and cost effective. Additionally, it is reported that ZnO can be synthesised into different shapes and sizes. Among the synthesised techniques are sputtering, chemical vapor decomposition, spin coating, spray pyrolysis, etc (Sutradhar & Saha, 2016). In another report was described zinc as a low cost material compared to indium or tin and it is mentioned that zinc oxide appears to be the least expensive TCO material for PV applications (Ghosh, Das, Banerjee, & Das, 2009).

Another research reported by Gao, Zhang, Zhang, and Xu (2011) in "Boron doped ZnO thin films fabricated by RF-magnetron sputtering", describes the deposition of pure ZnO and boron doped ZnO (ZnO:B) thin films on glass substrate using radio frequency-magnetron sputtering method. In this report it is mentioned a reduction in resistivity in ZnO:B compared with pure ZnO, $9.2 \times 10^{-3} \Omega\text{cm}$ and $6.3 \times 10^2 \Omega\text{cm}$ respectively. And an optical band gap of

3.38 eV for ZnO:B. Furthermore, they found that the crystal structure of pure ZnO and ZnO:B films have wurtzite structure (Gao, Zhang, Zhang, & Xu, 2011).

In this work, it is reported the production of zinc oxide films using spray pyrolysis method. Several works using this technique are well described, however in those reports complex and highly cost configurations are employed for deposition. This project describes the fabrication of transparent zinc oxide semiconductor films using a low cost spray pyrolysis configuration, never done before in Yachay Tech University. The obtained films were characterized using UV-vis, four probe measurements and Tauc plot method, showing an optical transmission of 95% in the visible range, an optical band gap of 3.26 eV and the lowest sheet resistance value of 6.7 k Ω .

0.1 Problem Statement

In the new technology of solar cells, the front surface electrode requires a transparent conductor. Nowadays, most of transparent conductors used are based on tin oxide, specifically indium tin oxide (ITO) films. However, ITO applications to photovoltaics represent a high cost due to it is based on indium, a scarce and expensive element (Kwon, Lee, & Kim, 2011). So, alternative materials cost-effective are needed in order to obtain a glass conductive and transparent films in visible region for possible applications in solar cells. In that sense, the present work describes a first approach in the realization of conductive and transparent glass plates based on zinc oxide.

0.2 General and Specific Objectives

0.2.1 General Objectives

1. Develop of glass transparent conductive ZnO and ZnO doped with boron films.
2. Measure of resistivity of the films using Four point probe method.
3. Measure the optical ban gap of the films using Tauc plot method.

0.2.2 Specific Objectives

1. Produce ZnO and ZnO boron doped films over glass substrates using ZnO and acetic acid solution by spray pyrolysis method.
2. Check the properties of the produced films at different boron doping concentrations.
3. Establish the resistivity in doped films as function of boron concentration by four point probe measurements.
4. Measure the optical band gap in ZnO undoped and ZnO boron doped films by Tauc plot method.

Chapter 1

Theoretical Background

1.1 Solar panels

Solar panels are solar devices composed by arrays of photovoltaics cells. This device convert solar energy directly from the sun to electric energy. Actually, in many countries as Germany, Japan, United States of America and others, the use of these devices have become very popular due to the ease of generating green energy for the daily use. Solar energy is available in abundance on the Earth and due to it is a renewable energy, it is an environmental friendly resource. However, manufacturing solar panels still being a large and highly cost process. Typically, solar panels manufacture starts with the formation of disc shaped silicon wafers. Then, these are cleaned to remove any impurity from the formation process. Once the cleaned process is finished, the silicon wafers are polished and doping agents are added to the silicon wafer modules in order to obtain the desired electrical properties. After this, These modules are spread on a matrix or a grid structure on the a flat sheet of solar panels. Commonly, solar panels are installed on the top of buildings to obtain the maximum solar energy from the sun, Figure 1.1(Bhatia, 2014).

1.2 Photovoltaics

Photovoltaics is the use of a semiconductor material that exhibits the photovoltaic effect for the generation of electrical power by the conversion of solar radiation (Pathakoti, Manubolu, & Hwang, 2018). Presently, materials as monocrystalline silicon, polycrystalline silicon, amorphous silicon, cadmium telluride, and copper indium gallium selenide/sulphide are used in photovoltaics (Bhatia, 2014). This method of electrical power generation employs solar panels containing a number of solar cells, where photons of light exciting electrons into a higher state of energy to act as charge carriers for an electric current.

For solar energy conversion, photovoltaic cells requires at least two different semiconductor layers. One layer with a positive charge and other with a negative charge, Figure 1.2. When photons from the light enter the cell, these are absorbed by the negative semiconductor material freeing electrons. The free electrons flow from the negative



Figure 1.1: Solar panels installed on the roof of a building. Reprinted from energy options, 2019.

layer through an external circuit to the positive layer producing an electric current. At certain level, a depletion zone is created between the p-n junction, this mean that there are no more charge carriers migration. Reprinted from Engineered Nanomaterials for Energy Applications, 2018.

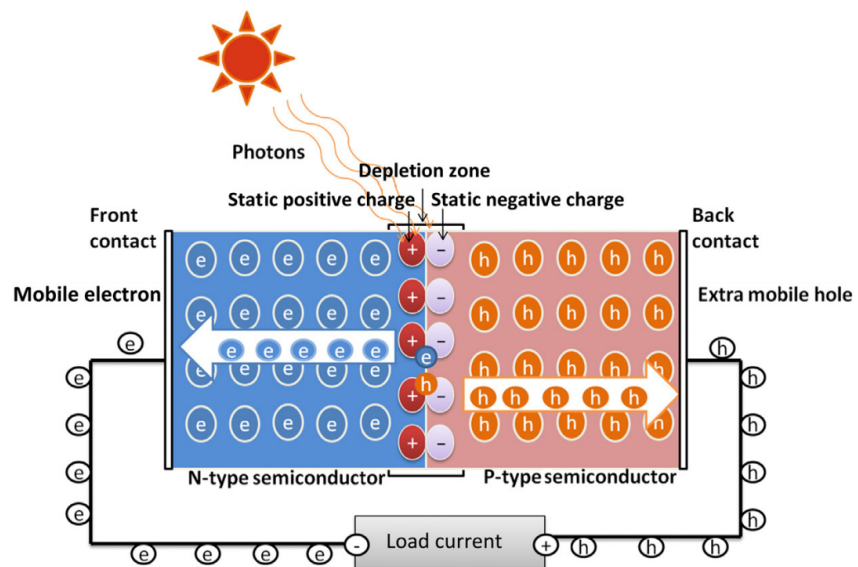


Figure 1.2: Schematic representation of a simple photovoltaic cell working. Reprinted from Engineered Nanomaterials for Energy Applications, 2018.

1.3 Optical band gap

One interesting property of semiconductors is their ability to manipulate electrical current as well as the ability to allow light to travel inside. "The conduction of electrical current is based on the flow of electrons"(Piprek, 2003). There are valence electrons (holes) and conduction electrons which are able to carry electrical current called carriers.

The separation between valence and conduction electrons is called energy gap. This is defined as the energy difference between the minimum valence band and the maximum conduction band (Piprek, 2003). In order to pass a valence electron to conductive electron, it needs to receive at least the gap energy and it will generate an electron-hole pair, Figure 1.3. On the other hand, energy is released as light by conduction electrons to become valence electrons. This valence electrons are in the outermost electron shell of the atom. In the case of semiconductors, the outer shell is fully occupied and the band gap energy is defined as the amount of energy required to dislodge an electron from its covalent bond, being this as a part of an electrical circuit (Bhatia, 2014). The energy necessary to promote an electron from the valence to the conductive band can be provided by light which is represented as energy packets called photons (Piprek, 2003).

To free an electron, photon energy must be greater enough as the band gap energy. However, photons with energies higher than the band gap, release the extra energy as heat when freeing electrons. So the key in PV is to convert into electricity the most of sunlight as possible (Bhatia, 2014).

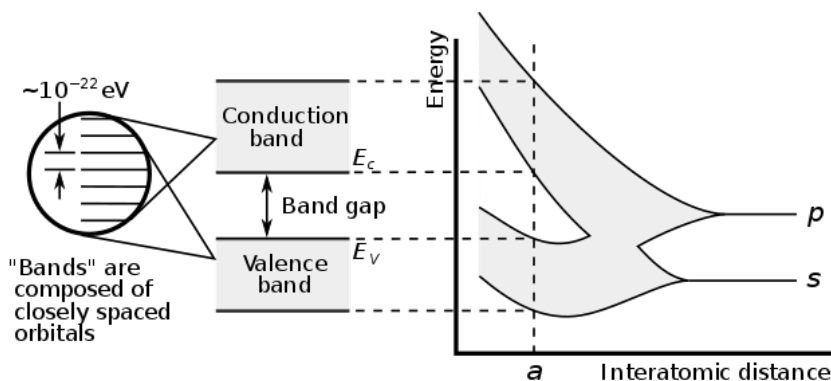


Figure 1.3: Schematic representation of an electronic band structure. At the center of the graph the energy levels are presented E_c (conduction band) and E_v (valence band). While at the right side atomic orbitals p and s are represented for separated atoms. Reprinted from Wikiwand, 2019.

In other sense, the band structure of the materials are described as an overlapping and coupling of the orbitals between atoms leading the formation of the filled lower valence band (binding states) and the empty upper conduction band (antibinding states) (Grundmann, 2006). And the band gap is defined as a range of energy where electronic states cannot exist (Grundmann, 2006).

1.4 Spray pyrolysis method

Spray pyrolysis is a simple and cost-effective technique which not requires high quality substrates or high cost equipment and allows the possibility to obtain films with large area (Ashour, Kaid, El-Sayed, & Ibrahim, 2006). It is employed a precursor solution and it is used for thin and thick films preparation. For this method the follow equipment is typically required: an atomizer, precursor solution, substrate heater, and temperature controller (Perednis & Gauckler, 2005).

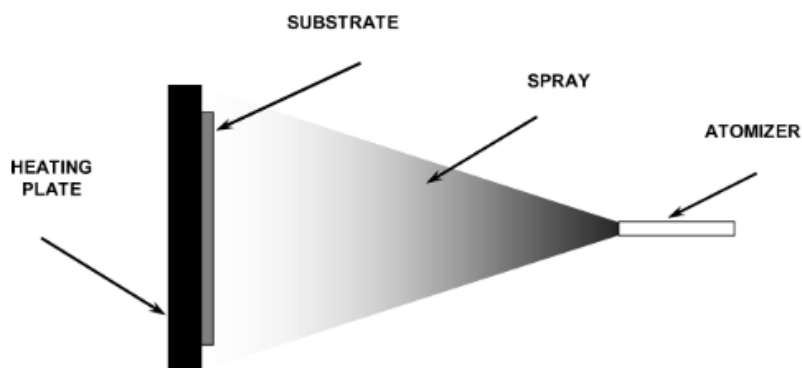


Figure 1.4: Schematic representation of spray pyrolysis technique. Reprinted from Thin Film Deposition Using Spray Pyrolysis, by D. Perednis & L. J. Gauckler, 2005, Zurich.

During the deposition process by spray pyrolysis method (Fig.1.4), a metal salt solution is sprayed onto a heated substrate. The substrate surface is impacted by droplets creating a disk shape structure and subjected to thermal decomposition to convert the metal salts into oxides. Parameters as pressure, droplets volume and substrate temperature affect the shape and size of the disk created. In order to create a film, multiple disks are overlapping onto the heated substrate (Perednis & Gauckler, 2005).

Perednis and Gauckler (2005) have described the influence of temperature in film morphology and properties. In many studies is reported that morphology of the film can change from a cracked to a porous micro structure by changing the temperature. Similarly, controlling the temperature, optical and electrical properties can be varied (Afify, Nasser, & Demian, 1991).

1.5 Two point versus four point probe

This method is used to measure the resistivity of semiconductors. The main problem of two point probe or two contact arrangement is that each contact serves as a current and as a voltage probe, Fig.1.5. This method looks easy due to its manipulation, however the interpretation of data is more complex. For example, if it is required the measure of the resistance of a device R_{dev} . Consider R_t as total resistance,

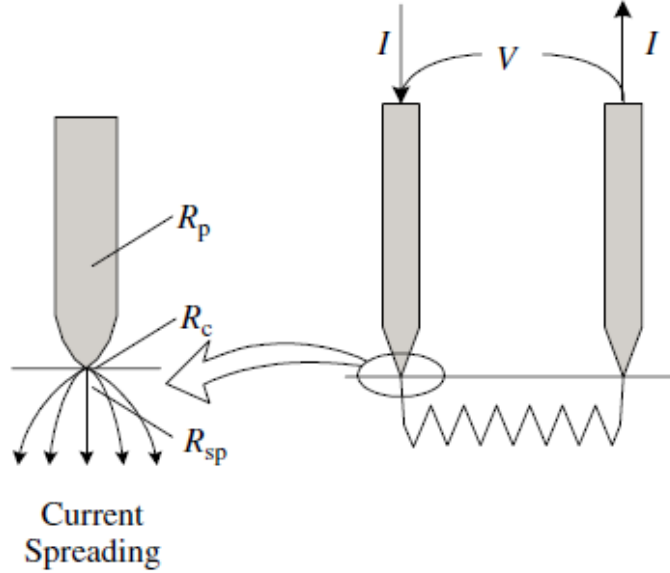


Figure 1.5: Two-point probe arrangement showing the probe resistance R_p , the contact resistance R_c , and the spreading resistance R_{sp} . Reprinted from SEMICONDUCTOR MATERIAL AND DEVICE CHARACTERIZATION, by D.K. Schroder, 2005, New Jersey.

$$R_t = \frac{V}{I} = 2R_w + 2R_c + R_{dev} \quad (1.1)$$

where R_w is wire or probe resistance, R_c contact resistance, and R_{dev} the resistance of the device under test. With this two probe method, it is not possible to distinguish those resistances from the obtained value of the two probe arrangement. So, as a solution for measure the resistance of the device R_{dev} is the four point probe or four contact arrangement. Now, in this configuration, the voltage is measured with two additional contacts. The principle of this configuration is that even that R_w and R_c still being part of the system, the current flowing through the voltage path is very low due to the high input impedance of the voltmeter. Hence, the voltage drops across R_w and R_c are negligibly small and can be neglected, so the measured voltage is basically the voltage drop across the device. Using this four probes, parasitic voltage drops are eliminated (Schroder, 2005).

Thin semiconductor layers are characterized by their sheet resistance R_{sh} , expressed in units of ohms per square. This sheet resistance is a measure of the resistivity averaged over the sample thickness subjected to the constrain $t \leq s/2$. The sheet resistance expression for a uniformly doped sample is given by

$$R_{sh} = \frac{\rho}{t} = \frac{\pi}{\ln(2)} \frac{V}{I} = 4.532 \frac{V}{I} \quad (1.2)$$

1.6 Tauc plot

Using the data obtained from optical transmission and absorption measurements is possible to determine the semiconductor band gap. Basically, the energy of the light determines how it is absorbed. For ideal UV-vis spectrum, photons with energies below the band gap are almost not absorbed, while photons with energies above the band gap are highly absorbed (Chen & Jaramillo, 2017). Thus, in absorption spectrum, the band gap represents the point at which absorption begins to increase, indicating the minimum amount of energy that an electron requires to be excited and the minimum photon's energy to be absorbed for a semiconductor material (Chen & Jaramillo, 2017).

Using UV-vis data, a estimation of the optical band gap following Tauc plot method is obtainable. This technique is based on the optical absorption strength which depends on the difference between the photon energy and the band gap, as is shown below:

$$(\alpha h\nu)^{1/n} = A(h\nu - E_g) \quad (1.3)$$

in the equation, h is Planck's constant, ν is the photon's frequency, α is the absorption coefficient, E_g is the band gap, and A is a proportionality constant. The value of the exponent n denotes the nature of the electronic transition as either direct or indirect and whether it is allowed or forbidden as is shown in Table 1.1:

Transition	Exponent
Direct allowed	$n=1/2$
Direct forbidden	$n=3/2$
Indirect forbidden	$n=3$
Indirect allowed	$n=2$

Table 1.1: Exponents used depending on nature of the electronic transition

In the case of direct transition, the conduction band minimum (CBM) coincide with the valence band maximum (VBM) in the k space (space of the wave vector), Fig. 1.6. So for the electronic transition from valence band (VB) to conduction band (CB) only a photon absorption is needed, it is described as two-particle interaction (electron and photon). On the other hand, for indirect transition, an additional particle is necessary to change the momentum of the electron (phonon), since the conduction band bottom not coincide with the valence band top, Fig. 1.6, for this reason this transition is described as three-particle interaction (photon, electron, phonon)(Wooten, 1972)(Chen & Jaramillo, 2017).

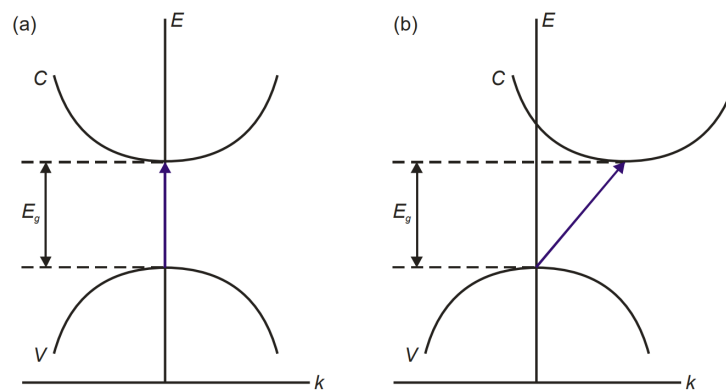


Figure 1.6: Interband transitions. A direct transition diagram from valence band V maximum to conduction band C minimum (a) and an indirect transition diagram from valence band maximum to conduction band minimum (b). In the diagram E_g is the band gap. Reprinted from OPTICAL PROPERTIES OF SOLIDS, by F. Wooten, 1972.

Chapter 2

Methodology

2.1 Spray Pyrolysis Method for Fabrication of Transparent Conductive Glass Films

The spray pyrolysis method was used to the deposition of zinc oxide over glass substrate. For this a solution of zinc oxide in acetic acid was prepared. The solution was prepared mixing 8.1 g of zinc oxide diluted in 44.8 ml of acetic acid (30%) and distilled water was added until to reach 100 ml of solution. Then, the aqueous solution was mixed by a magnetic stirred until completely dissolve all white powder, obtaining a final transparent solution. The volume used for each deposition was 35 ml.

For zinc oxide boron doped films, a similar process as described before was employed. However, for this part, boron acid was used as boron doping precursor. In this section, different percentages of boron were used in order to analyze their effects (sheet resistance, band gap, and transparency) in the final films. Same zinc oxide content was added 8.1g to 44.8 ml of diluted acetic acid (30%) and 55.2 ml of distilled water. The doping levels of boron in ZnO are 0.49 wt %, 0.98 wt %, and 4.41 wt %. For each deposition 35 ml of solution was spun over a cleaned glass substrate.

The final solution was sprayed onto a heated substrate using compressed air as a gas carrier. For this, a gravity airbrush and a "SURTEK" air compressor were used to spray the solution. The solution deposition was done at low air pressure and low content release. For this work, a station of deposition was set up. This station consist of a gas industrial burner with a steel plate over it, fig. 2.1. The steel plate was used as a supporter base for the substrate employed. The temperature was controlled with a thermocouple screwed to the steel plate. Microscope glass slides were used as substrate (2.54 X 7.62 cm and thickness 1-1.2 mm) over a gas heater for deposit ZnO films. The temperature was controlled regulating the gas flow using a valve.

Different conditions were tested during deposition process, however, due to the instruments employed do not present approximated regulation values, just perceived conditions by the operator can be described with respect to the spray used. During the deposition, three different solution flows were used (low flow, moderate flow and high

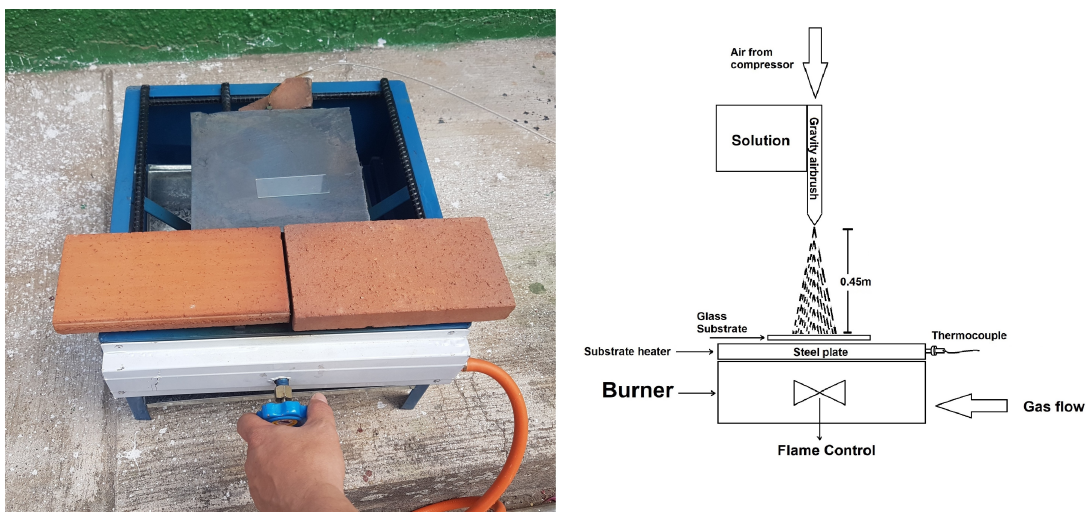


Figure 2.1: Burner used with the steel plate to support the substrate. Behind the steel plate is screwed a thermocouple to estimate the temperature of the plate.

solution flow) in order to observe the effect in optical and electrical properties. Another controlled factor was the carrier gas, this was controlled by a pressure regulator included in the gravity airbrush. Due to a low pressure employed during the deposition, the nozzle of the airbrush to the glass substrate distance was approximately 0.45 m as is shown in Figure 2.1. The low pressure used was in order to avoid the movement of the glass substrate over the heat plate.

The heat plate was kept between 400 and 450 °C. Several papers report that best results have been obtained at substrate temperature higher than 400 °C. In effect, Aktaruzzaman, Sharma, and Malhotra (1991) mention the influence of substrate temperature with transmission, obtaining as highest transmission value of 85% around 400 °C, and small transmission effects with higher temperatures until 500 °C. So, for the deposition process, the temperature was fixed into the range reported.

2.2 Four point probe measurements

The resistivity of semiconductors can be measured by this method. In this configuration, the voltage is measured with four contacts as is shown in Figure 2.2. For this, the four probes are separated by same distances one probe to the other. As the four point probe device was fabricated in Yachay Tech University laboratories specifically for this research purpose, the four probes were welded in a universal printed circuit board separating each probe from the other 2.54 mm with linear symmetry. Then, the probes which will supply the constant current (1 and 4 in Figure 2.2) are connected at the endings, while the probes connected to the voltmeter (2 and 3 in Figure 2.2) are placed between the current probes. To obtain the resistance of the device, a constant current is applied to the outer probes and the

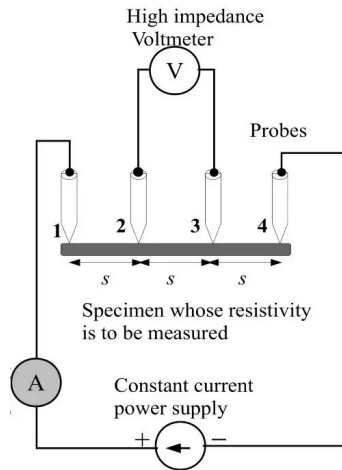


Figure 2.2: Four-point probe method for resistivity measurements of a specimen. Reprinted from the Quora, Electronic batteries Post, 2017.

voltage variation value is measured with the inner probes. The measurements were visualized with the use of two digital Dt832 multi-meters. The sensibility of the four point probe device for current is between 10 nA to 1 mA and for electric tensions between 10 mV to 100 V. The fabricated device is shown in Figure 2.3.

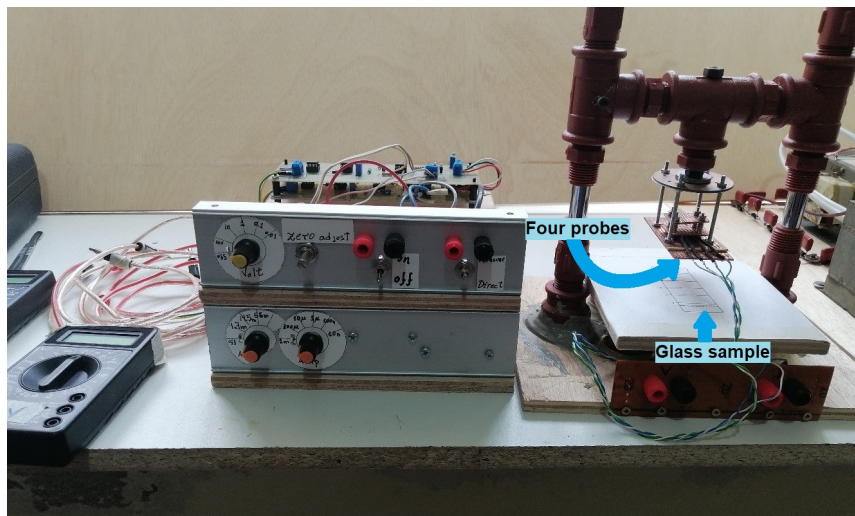


Figure 2.3: Four-point probe device fabricated in Yachay Tech University for this research work.

Thin semiconductor layers are characterized by their sheet resistance R_{sh} , expressed in units of ohms per square. This sheet resistance is a measure of the average resistivity over the sample thickness subjected to the constrain

t (thickness) $\leq s$ (probes separation)/2. Then, the sheet resistance expression for a uniformly doped sample is given by

$$R_{sh} = \frac{\rho}{t} = \frac{\pi}{\ln(2)} \frac{V}{I} = 4.532 \frac{V}{I} \quad (2.1)$$

In this work, as the uniformity of the film is also desired to know, five sheet resistance measurements were taken from the sample on the regions shown in Figure 2.4. The uniformity of the deposited films were estimated calculating standard deviation values considering the five sheet resistance measurements obtained from each deposited layer. For each group (ZnO, ZnO:B 0.49 wt% and ZnO:B 0.98 wt%) nine samples were performed.

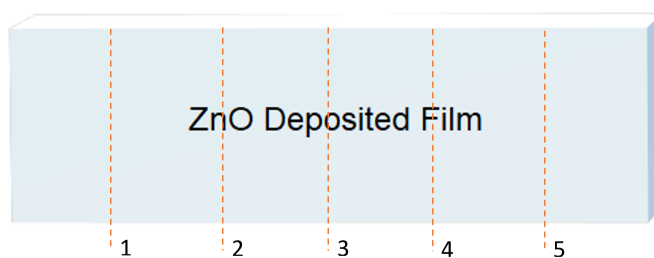


Figure 2.4: Sections in which films were differentiated in order to estimate the homogeneity of the deposition for each film. The dotted lines represent the places where the four point probe measurements were taken. In table 3.1 is presented an average of these 5 measurements.

2.3 Measurements of optical band gap using Tauc plot method

In semiconductors, the optical band gap can be estimated by UV-vis spectroscopy method. During this process, a source of light passes through the sample and transmitted light is measured as a functions of wavelength. Typically, a spectra is presented by light wavelength units rather than its energy. So, their conversion from wavelength (nm) to energy (eV) units are achieve as follow:

$$hv[eV] = \frac{hc}{\lambda} = \frac{1239.8[eV * nm]}{\lambda[nm]} \quad (2.2)$$

where h is the Planck's constant in [$eV * s$], c is the speed of light in [$nm * s^{-1}$], and λ is the wavelength in [nm].

For these measurements, a UV-vis device was fabricated based on the requirements for this research purpose. Basically, it consists of a detector, a light source and a wood holder for the microscope glass where the ZnO films were deposited. The data obtained from the device was collected using "SpectraGryph 1.2-spectroscopy software", where transmittance and reflection measurements were able. This UV-vis spectrometer fabricated in Yachay Tech University has a optimal working range between 350 to 950 nm. A previous calibration before any measurement is required, for this, a mercury lamp is employed. The UV-vis device fabricated is shown in Figure 2.5.

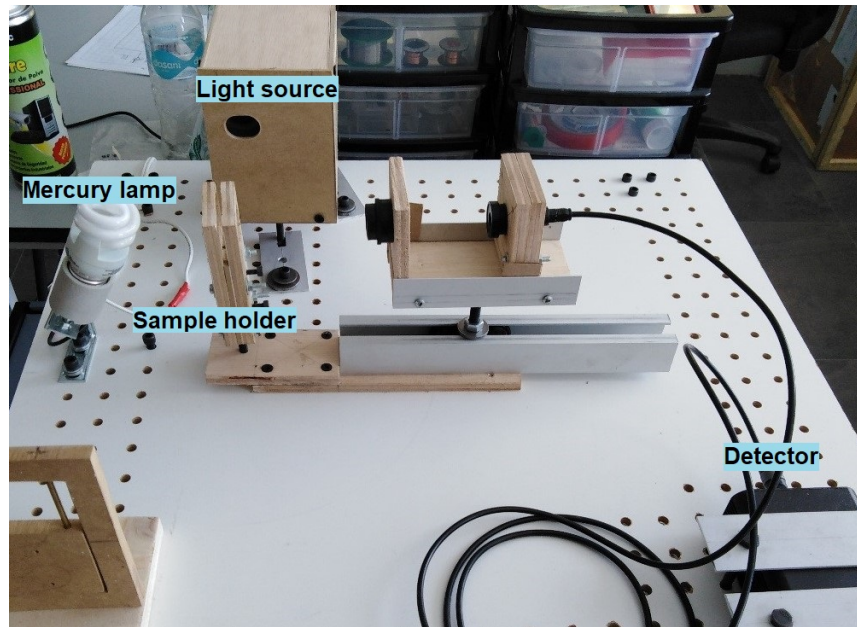


Figure 2.5: UV-vis device fabricated in Yachay Tech University for this research work.

Using the data obtained from optical transmission and absorption measurements is possible to determine the semiconductor band gap. In absorption spectrum, the band gap represents the point at which absorption begins to increase. Applying Tauc plot method to the data collected from UV-vis a estimation of the optical band gap is obtainable. First, the optical absorption strength as a function of the photon energy is plotted, in this case "OriginPro 2017" was used. This graph is associated with the following equation, being the left side of the equation the Y axis of the plot:

$$(\alpha h\nu)^{1/n} = A(h\nu - E_g) \quad (2.3)$$

in the equation, h is Planck's constant, ν is the photon's frequency, α is the absorption coefficient, E_g is the band gap, and A is a proportionality constant. The value of the exponent n denotes the nature of the electronic transition as either direct or indirect and whether it is allowed or forbidden:

- for direct allowed transitions: $n=1/2$,
- for direct forbidden transitions: $n=3/2$,
- for indirect forbidden transitions: $n=3$.
- for indirect allowed transitions: $n=2$,

In general, absorption is dominated by allowed transitions, leaving $n=1/2$ or $n=2$ as is shown in table 1.1, for direct and indirect transitions, respectively. In order to obtain the band gap following Tauc plot analysis, the optical absorbance data is obtained in a range below and above the band gap. Then, a plot of $(\alpha h\nu)^{1/n}$ versus $(h\nu)$ provides

a linear region, where through extrapolation in this section, the interception with photon energy axis will give the band gap value (Viezbicke, Patel, Davis, & Birnie, 2015).

Chapter 3

Results & Discussion

3.1 Band Gap Obtained by Tauc Plot Method

For this section UV-vis transmittance and reflectance measurements were performed using "SpectraGryph" which is a spectroscopy software used to obtain the mentioned spectrum. The spectrophotometer was calibrated using a mercury lamp and the transmission spectra was measured in the region between 350 to 950 nm. With reflectance and transmittance measurements, the optical energy band gap was calculated using Tauc plot method. In order to obtain the absorption coefficient (α) used in Tauc plot, it is necessary a rough approximation described by Benno and Joachim (2003), in "Optical Properties of Thin Semiconductor Films", where it is presented a relation for calculate the absorption coefficient in base of reflectance (R), transmittance (T), and thickness of the film d . The equation to calculate is:

$$R + T = e^{\alpha d} \quad (3.1)$$

and solving for α , it is obtained,

$$\alpha = \ln(R + T) \frac{1}{d} \quad (3.2)$$

Using Equation 3.2 and replacing in the relation shown in equation 2.3, it is possible to plot one of the axis. For the photon energy axis, the spectrum obtained is given as a function of wavelength, so Equation 2.2 is used for the conversion from wavelength (nm) to energy (eV) units. Finally to obtain Tauc plot, it is defined the exponent value n as direct allowed transition $n = 1/2$ as is shown in Table 1.1. This considering that plotting for all kind of transitions the graph that best matches is for direct allowed transition which additionally, this is consistent with Kumar, Singh, Purohit, and Mehra (2011), where a direct band gap transition is described for zinc oxide semiconductor.

Once ($\lambda h\nu$) versus photon energy is plotted, a straight line is drawn in the region of the graph that best matches with a linear behaviour. This is because the plot is basically a representation of the absorption coefficient as a function of photon energy, which means that at values equal and higher than the optical band gap, the photon energies will be highly absorbed by the semiconductor material. Thus, the intersection between the line with the photon energy

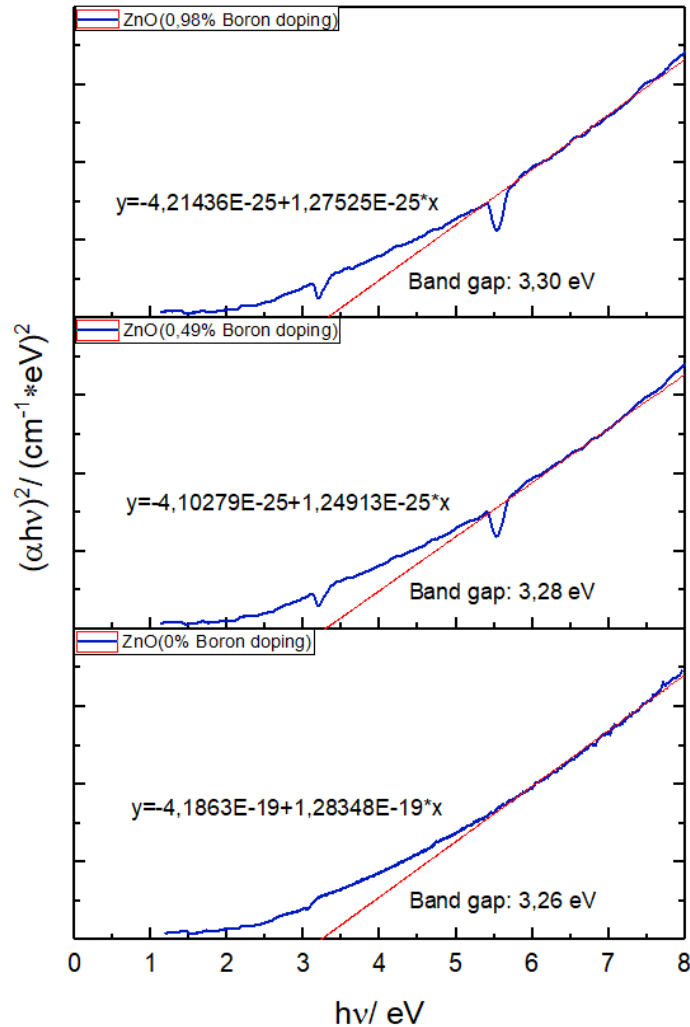


Figure 3.1: Tauc plot of zinc oxide films boron doped at different concentrations. From the bottom to the top graph: 0%, 0.49%, and 0.98% boron doped respectively. Absorption coefficients by $(h\nu)$ as a function of eV are plotted in blue. Red lines are the extrapolation in the linear region of the spectra and their intersection with photon energy axis correspond to the best estimated optical band gap value.

axis defines the optical band gap of the deposited material. Figure 3.1 shows the obtained results applying Tauc plot method to three different films belonging to the ZnO undoped group, ZnO:B 0.49 wt% group and ZnO:B 0.98 wt% group. The Tauc plot of the group with the highest boron doping (ZnO:B 4.41 wt%) is not presented due to the objective of this work is the fabrication of transparent conducting films, and all of the films deposited in this group showed an opaque color and any transparent film was formed. Additionally, the most of the samples of this group,

during the deposition process, the glass substrate broke. So, UV-vis measurements were not performed for this group. On the other hand, the presented graph shows the optical band gap obtained for each of the other groups. Even that for each group nine samples were deposited, the Tauc plot obtained in the nine samples of each group do not vary too much among the presented graphs. Moreover, in the Figure 3.1 can be observed from the results a small variation in the band gaps obtained at different concentrations of boron. While the percentage of boron doping increases, the optical band gap also increases. The optical band gap of the ZnO:B 0.98 wt% shows the highest value with 3.30 eV, for ZnO:B 0.49 wt% the value obtained was 3.28 eV, while the ZnO without doping agents presented the lowest band gap value 3.26 eV. These small differences are in good agreement with reported values for ZnO semiconducting thin films. The increment of the semiconductor band gap for doped material is described by Burstein-Moss effect where the increment in band gap value is due to an increase in carrier concentrations. Generally, the Fermi level of semiconductors lies between the conduction and valence band, but when the material is doped, electrons populate all states close to the conduction band which push the absorption edge to higher energies, this as effect pushes the Fermi level inside the conduction band. To promote an electron from the valence band to conduction band, generally, it occurs above the Fermi level, but considering that now all states below Fermi level are occupied, Pauli's exclusion principle forbids the promotion of these electron to the occupies states. Due to this effect, the observed band gap increases. Ravindran (2013) mentions that, " this effect occurs when the electrons carrier concentration exceed the conduction band edge density of states".

3.2 Transmission measurements

For this section UV-vis spectrometer and "SpectraGryph" software were employed to analyze transmittance of zinc oxide films. The spectrometer was calibrated using a mercury lamp and all measurements were performed at room temperature.

Figure 3.2 shows the percentage transmission spectra for ZnO undoped and ZnO doped film at different boron concentrations. It is observed a high transmission in visible range for these films with a 95% as the highest value. Also, in this figure is observed a decrease in transmittance % in the range below 380 nm approximately, which is consistent with the optical band gap 3.26-3.30 eV shown in Fig. 3.1. This means that from this point, the photon energy fulfill with the minimum energy required to promote an valence electron to the conduction band, so photons with energies higher than the optical band gap will be absorbed. This event is represented as a decrease in transmission. The relation between wavelength and photon energy is described by the Equation 2.2. Considering this equation, lower wavelengths are more energetic than higher wavelengths. As absorption increases for values with higher energies than the optical band gap presented in Figure 3.1, for this reason the transmission decreases more below 380 nm and not above this point as can be seen in Figure 3.2. In order to obtain the corresponding wavelength to the associated photon energy, the Equation 2.2 can be used.

Changes in transparency in deposited films at different boron doping concentration was perceived visually compared among the films. In Fig. 3.3, it can be observed that for highest doping concentration (4.41 wt%) film the lines drawn over the paper almost disappear, while for doping concentrations below 1 wt % the transparency keeps similarly between them. Not much difference is observed. This fact matches with Figure 3.2, where the transmission

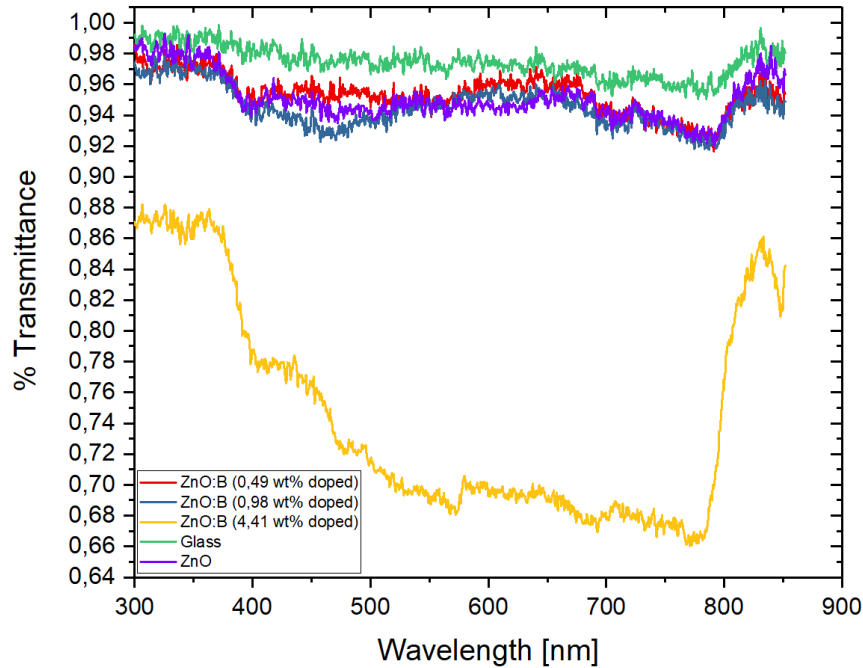


Figure 3.2: Optical transmission percentage for ZnO and ZnO 0.49, 0.98, 4.41 wt% boron doped film. In green the transmission spectrum of the glass substrate used for ZnO deposition.

spectrum for ZnO and ZnO boron doped below 0.98 have similar behaviour. While for ZnO with 4.41 boron doping concentration is opaque in Figure 3.2, showing that most of the visible light is reflected.

3.3 Sheet resistance values

Averaged sheet resistance values [$k\Omega$]										
Film number	1	2	3	4	5	6	7	8	9	Average
ZnO (0 wt% doped)	143,9	34,8	661,0	368,6	209,4	424,1	112,5	62,4	248,5	251,7
ZnO:B (0,49 wt% doped)	341,0	344,8	264,9	139,1	369,3	293,8	13,3	6,7	11,5	198,3
ZnO:B (0,98 wt% doped)	401,0	186,8	148,7	288,4	187,2	105,3	25,3	25,5	12,2	153,4

Table 3.1: Averaged sheet resistance values presented in [$k\Omega$] units for each deposited film, in order to know the lowest resistance at different wt% boron doping.

Using four probe technique, the sheet resistance values of the films were measured. All measurements were carried out at room temperature. The data collected from these measurements are presented in Table 3.1. The

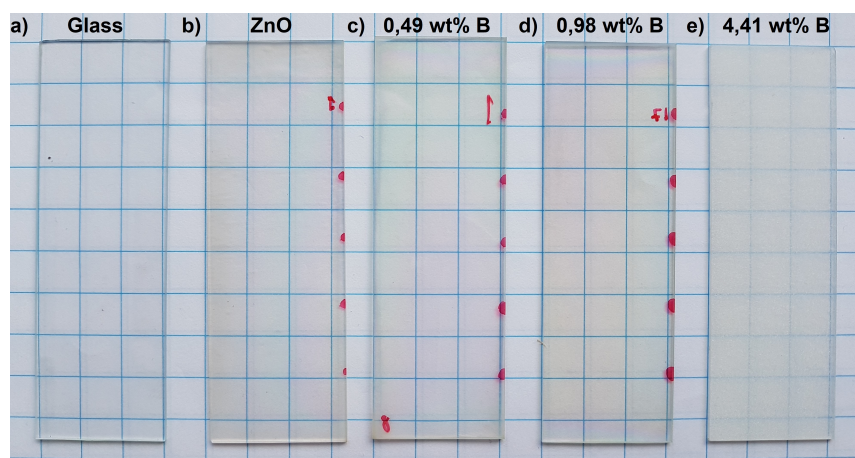


Figure 3.3: Obtained films at different boron doping concentrations. Glass substrate as reference a), ZnO without doping b), ZnO with 0.49 wt% boron doping c), ZnO with 0.98 wt% boron doping d), and ZnO with 4.41 wt% boron doping e).

minimum value observed of sheet resistance is $6.7 \text{ k}\Omega$, while the highest value obtained is $661.0 \text{ k}\Omega$. The minimum value measured correspond to 0.49 wt % boron doped film. And the maximum value correspond to ZnO film without doping. In the other hand, focusing in general sheet resistance values for each group, the average sheet resistance obtained in 0.98 wt% boron doped correspond to the lowest value measured $153.4 \text{ k}\Omega$, while in ZnO without doping, the sheet resistance value is still the highest with $251.7 \text{ k}\Omega$. Showing a trend to reduce the sheet resistance values when the boron doping concentration increases, this is more appreciable in Fig. 3.4. Generally, ZnO semiconductor without doping is described as a n-type semiconductor, this due to the formation of donors by oxygen vacancies and interstitial zinc atoms as is described by Ashour, Kaid, El-Sayed, and Ibrahim (2006). Nevertheless, when ZnO films are doped with a trivalent cation, in this case boron, the carrier density increases, resulting in a decrease of ZnO resistivity as it is observed in Table 3.1 and Figure 3.4 for ZnO Boron doped 0.49 and 0.98 wt% (Min, 2003).

Uniformity of the films										
Film number	Standard Deviation									Average
	1	2	3	4	5	6	7	8	9	
ZnO (0 wt% Boron doped)	37,7	25,6	20,8	24,2	81,0	81,9	40,0	60,5	67,0	48,7
ZnO (0,49 wt% Boron doped)	71,2	82,4	42,8	57,6	51,1	68,6	9,2	0,3	3,4	43,0
ZnO (0,98 wt% Boron doped)	50,9	28,1	19,3	66,6	56,6	20,0	2,0	3,4	0,8	27,5

Table 3.2: Standard deviation values for sheet resistance measurements of each film, in order to know the homogeneity deposition at different wt% boron doping.

Using the sheet resistance values and checking its standard deviation, the homogeneity of the deposited film

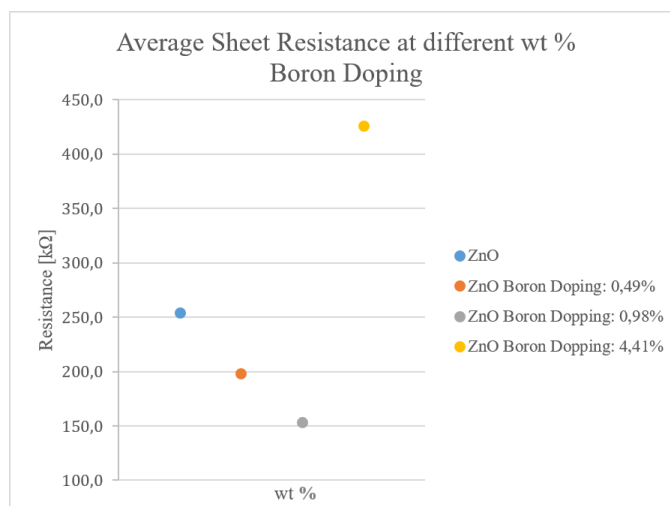


Figure 3.4: Representation of sheet resistance values at different doping levels. The resistance values are presented in $k\Omega$. A clear trend in sheet resistance values is observed while the doping level increases, the Sheet resistance decreases until a certain point of doping where sheet resistance increases.

over entire surface substrate was studied. For this, five measurements of sheet resistance were done to each of the nine slides corresponding to each one of the groups (ZnO undoped, ZnO:B 0.49 wt% and ZnO:B 0.98 wt%). Then the standard deviation was calculated between the five sheet resistance measurement for each of the nine deposited films. The calculated standard deviation values for each deposited film and the average standard deviation value for each group is presented in Table 3.2. As it was mentioned before, the objective of this work is to fabricate transparent films, and due to the films of the group ZnO:B 4.41 wt% are not transparent, most of the films during deposition broke and the sheet resistance measurements could not be performed due to their high resistance, the measurement of this groups are not presented. The five sheet resistance measurements done to each slide were taken in different places over the deposited film as is shown by dotted lines in Fig. 2.4. It is observed in Table 3.2, that the highest standard deviation values in sheet resistant correspond to ZnO not doped films, indicating how they differ in homogeneity between their sections. Also, it is observed a reduction in standard deviation values for zinc oxide doped films, showing an increase in homogeneity in the films surface when the wt% of boron doping is increased. However, when the percentage of boron doped was raised to 4.41 wt %, a reduce in homogeneity and an increase in sheet resistance values was observed as is shown in Fig. 3.4. In this figure, the average sheet resistance value for the group of ZnO:B 4.41 wt% was calculated just from three samples of this group due to it was not possible to measure in the other samples. In "Influence of substrate temperature on the structural, optical and electrical properties of ZnO thin films prepared by spray pyrolysis", by Afify, Nasser, and Demian (1991), is reported that the increase in sheet resistance values is due to a high increase of carriers concentration which reduces carriers mobility. So, in this case the increment in doping agents is too high at the point that reduces the mobility of the carries in the films, due to this effect, higher sheet resistance values are measured at very high doping concentrations.

In addition, during the deposition it was observed that the transparency of films reduces when the solution flow increases. On the other hand, very low flows increases the transparency of the films and increases the sheet resistance measurements. So a moderate flow is required in order to obtain good transparency and low sheet resistance values. In "Physical properties of ZnO thin films deposited by spray pyrolysis technique", by Ashour et al. (2006), is mentioned that the resistivity of ZnO films depends the solution flow rate. Which is consistent with the observations obtained during the deposition process.

Chapter 4

Conclusions & Outlook

Reproducible ZnO and ZnO boron doped thin films have been obtained over a glass substrate by spray pyrolysis technique. This was confirmed using Tauc plot method obtaining an optical band gap of 3.26 for ZnO films, which is consistent with optical band reported for this material in previous works. Using spray pyrolysis technique, these films were performed with a relative low cost of production, considering the equipment employed and the substances used. Optical and electrical measurements were conducted showing different results depending of boron doped concentration. For ZnO films an average sheet resistance measured was 251.7 k Ω , while for ZnO 0.49 wt% boron doped was 198.3 k Ω , and for ZnO 0.98 wt% the resistance values was 153.4 k Ω being the lowest with respect the other films, demonstrating that with an increase in doping agents below 1 wt% the conductivity of the film can be improved. Also, a high transmission around 95% was achieved by boron doping. Variations in optical band gap were measured using Tauc plot method. It was observed small variations in the direct optical band gap depending of the boron doping concentration, while the concentration of boron increases the optical band gap also increases.

Further work is required in order to improve the fabrication process and to obtain ZnO thin films with specific characteristics depending on the application. For this, a better control of ZnO deposition by spray pyrolysis method is required. The conductivity of ZnO films were tested as a function of wt% boron doping, a relation with its concentration it was found. Optical and electrical properties using different doping agents in ZnO films should be studied. Also, composition analysis is required in order to quantify the amount of boron present in deposited layers, this analysis would allowed to improve the relation of the boron concentration with optical an electrical properties. Among some properties showed by ZnO films such as high optical transparency in visible and near-infrared region and controlling resistance together with its large abundance make ZnO as a promising material between all oxides for potential application in solar cells as transparent conductive thin film. This considering, also, that actually some projects are developed in Ecuador oriented to renewable energies, one example is the implementation of photovoltaics in Galapagos islands and in Amazon region. So, this project is one of the steps to bring us closer to other possible implementation of clean energy in Ecuador.

Bibliography

- [1] (2018). Engineered Nanomaterials for Energy Applications. In *Handbook of Nanomaterials for Industrial Applications*, pages 751–767. Elsevier.
- [2] Administration, U. S. E. I. (2019). International Energy Outlook 2019 with projections to 2050. Technical report.
- [3] Afify, H. H., Nasser, S. A., and Demian, S. E. (1991). Influence of substrate temperature on the structural, optical and electrical properties of ZnO thin films prepared by spray pyrolysis. *Journal of Materials Science: Materials in Electronics*, 2(3):152–156.
- [4] Aktaruzzaman, A., Sharma, G., and Malhotra, L. (1991). Electrical, optical and annealing characteristics of ZnO:Al films prepared by spray pyrolysis. *Thin Solid Films*, 198(1-2):67–74.
- [5] Aranovich, J., Ortiz, A., and Bube, R. H. (1979). Optical and electrical properties of ZnO films prepared by spray pyrolysis for solar cell applications. *Journal of Vacuum Science and Technology*, 16(4):994–1003.
- [6] Ashour, A., Kaid, M., El-Sayed, N., and Ibrahim, A. (2006). Physical properties of ZnO thin films deposited by spray pyrolysis technique. *Applied Surface Science*, 252(22):7844–7848.
- [7] Bhatia, S. (2014). Energy resources and their utilisation. In *Advanced Renewable Energy Systems*, pages 1–31. Elsevier.
- [8] Chen, Z. and Jaramillo, T. F. (2017). The Use of UV-visible Spectroscopy to Measure the Band Gap of a Semiconductor. Technical Report 10, Stanford University.
- [9] Djurišić, A. B., Liu, X., and Leung, Y. H. (2014). Zinc oxide films and nanomaterials for photovoltaic applications. *Physica Status Solidi - Rapid Research Letters*, 8(2):123–132.
- [10] Gao, L., Zhang, Y., Zhang, J. M., and Xu, K. W. (2011). Boron doped ZnO thin films fabricated by RF-magnetron sputtering. *Applied Surface Science*, 257(7):2498–2502.
- [11] Ghosh, B., Das, M., Banerjee, P., and Das, S. (2009). Fabrication of the SnS/ZnO heterojunction for PV applications using electrodeposited ZnO films. *Semiconductor Science and Technology*, 24(2).

- [12] Gordon, R. G. (1997). Deposition of transparent conducting oxides for solar cells. In *AIP Conference Proceedings*, volume 394, pages 39–48. AIP.
- [13] Grundmann, M. (2006). *The physics of semiconductors: An introduction including devices and nanophysics*. Springer Berlin Heidelberg.
- [14] Hosono, H. (2013). New Frontiers Opened Up Through Function Cultivation in Transparent Oxides. In *Handbook of Advanced Ceramics: Materials, Applications, Processing, and Properties: Second Edition*, pages 455–487. Elsevier.
- [15] IRENA (2015). Renewable Energy Policy Brief Ecuador. (June):10.
- [16] Kumar, V., Singh, R., Purohit, L., and Mehra, R. (2011). Structural, Transport and Optical Properties of Boron-doped Zinc Oxide Nanocrystalline. *Journal of Materials Science & Technology*, 27(6):481–488.
- [17] Kwon, J.-Y., Lee, D.-J., and Kim, K.-B. (2011). Review paper: Transparent amorphous oxide semiconductor thin film transistor. *Electronic Materials Letters*, 7(1):1–11.
- [18] Min, Y. M. I. o. T. (2003). *Properties and Sensor Performance of Zinc Oxide Thin Films*. PhD thesis, Massachusetts Institute of Technology.
- [19] Nagar, S. and Chakrabarti, S. (2017). *Optimisation of ZnO thin films: Implants, properties, and device fabrication*. Springer Singapore, Singapore.
- [20] Pathakoti, K., Manubolu, M., and Hwang, H.-M. (2018). Nanotechnology Applications for Environmental Industry. In *Handbook of Nanomaterials for Industrial Applications*, pages 894–907. Elsevier.
- [21] Perednis, D. and Gauckler, L. J. (2005). Thin film deposition using spray pyrolysis. *Journal of Electroceramics*, 14(2):103–111.
- [22] Petrova-Koch, V., Hezel, R., and Goetzberger, A., editors (2020). *High-Efficient Low-Cost Photovoltaics*, volume 140 of *Springer Series in Optical Sciences*. Springer International Publishing, Cham.
- [23] Piprek, J. (2003). *Semiconductor Optoelectronic Devices*. Elsevier.
- [24] Scharber, M. C., Mühlbacher, D., Koppe, M., Denk, P., Waldauf, C., Heeger, A. J., and Brabec, C. J. (2006). Design Rules for Donors in Bulk-Heterojunction Solar Cells—Towards 10 % Energy-Conversion Efficiency. *Advanced Materials*, 18(6):789–794.
- [25] Schroder, D. K. (2005). *Semiconductor Material and Device Characterization*. John Wiley & Sons, Inc., Hoboken, NJ, USA.
- [26] Suganthi, L. and Samuel, A. A. (2012). Energy models for demand forecasting—A review. *Renewable and Sustainable Energy Reviews*, 16(2):1223–1240.

-
- [27] Sutradhar, P. and Saha, M. (2016). Green synthesis of zinc oxide nanoparticles using tomato (*Lycopersicon esculentum*) extract and its photovoltaic application. *Journal of Experimental Nanoscience*, 11(5):314–327.
- [28] Viezbicke, B. D., Patel, S., Davis, B. E., and Birnie, D. P. (2015). Evaluation of the Tauc method for optical absorption edge determination: ZnO thin films as a model system. *physica status solidi (b)*, 252(8):1700–1710.
- [29] Vinet, L. and Zhedanov, A. (2010). A "missing" family of classical orthogonal polynomials. *Antimicrobial agents and chemotherapy*, 58(12):7250–7.
- [30] Wooten, F. F. (1972). *Optical properties of solids*. Academic Press, New York.

Abbreviations

ARCONEL Control Electricity Agency 2

CB conduction band 12

CBM conduction band minimum 12

CONELEC National Electric Council 2

EIA Energy Information Administration iii

ITO indium tin oxide 5

PV photovoltaic 1

TCO transparent conductive oxide 3

VB valence band 12

VBM valence band maximum 12

ZnO zinc oxide 3